Conceptual design of a $Cs_2LiLaBr_6$ scintillator-based neutron total cross section spectrometer on the Back-n beam line at CSNS

Dajun ZHAO,[1] Song FENG,[1, *] Pinjing CHENG,[1] Rong LIU,[2] Wen LUO,[1] Haoqiang WANG,[1] Jieming XUE,[1] Kun ZHU,[1] and Bo ZHENG[1]

[1]*School of Nuclear Science and Technology, University of South China, Hengyang 421001, China*
[2]*Institute of Nuclear Physics and Chemistry, China Academy of Engineering Physics, Mianyang 621900, China*

In order to reduce the experimental uncertainty in the ^{235}U resonance energy region and improve the detection efficiency for neutron total cross section measurements compared with the neutron total cross section spectrometer (NTOX), a dedicated lithium-containing scintillation detector has been considered to be developed on the Back-n beam line at the China Spallation Neutron Source (CSNS). The FAst Scintillator-based neutron Total cross section (FAST) spectrometer has been designed based on a $Cs_2LiLaBr_6$ (CLLB) scintillator considering the γ-ray flash and neutron environment on the Back-n beam line. Response of the CLLB scintillator to neutrons and γ-rays has been performed with different ratios of ^{6}Li/^{7}Li abundance using Geant4. The neutron-γ discrimination performance of the CLLB has been simulated considering different scintillation parameters, physical designs and light readout modes, respectively. A cubic ^{6}Li-enriched ($> 90\%$) CLLB scintillator, which has a thickness of 4-9 mm and a side length no less than 50 mm to cover the Φ50 mm neutron beam at the spectrometer position, has been proposed coupling to a side readout SiPM array for the construction of the FAST spectrometer. The developed simulation techniques in neutron-γ discrimination performance could provide technical support for other neutron-induced reactions measurement on the Back-n beam line.

Keywords: Neutron total cross section, CLLB scintillator, Geant4, Pulse shape discrimination(PSD).

I. INTRODUCTION

The neutron total cross section is a basic quantity describing the sum of probabilities of interactions between an incident neutron and a nucleus in an unit target area [1]. It plays a significant important role in the development of nuclear energy systems [2] and in fundamental nuclear physics [3]. Pulsed white neutron sources and advanced spectrometers are essential for measuring high quality neutron total cross sections. The Back-n white neutron beam line, which utilizes the back-streaming neutrons through the incoming proton channel at the spallation target station of the China Spallation Neutron Source (CSNS) [4, 5], could deliver high intensity neutrons with energy spectrum spanning from 0.5 eV to 200 MeV. A good time resolution related to the time-of-flight (TOF) measurements makes Back-n a merit platform for neutron-induced cross section measurements with high accuracy in a wide energy range. The current neutron total cross section spectrometer installed on the Back-n beam line is NTOX, which is based on a multi-cell fission chamber with a maximum of 8 ^{235}U and ^{238}U cells [6, 7] and has successfully been applied for neutron total cross section measurements[8–10].

The neutron total cross section is usually obtained by measuring the neutron flux with and without the sample for the neutron transmission determination at a certain energy together with considering the sample thickness and nuclei density. A pulsed neutron source combined with the TOF technique allows neutron total cross section data to be measured over a wide energy range. The fission cross section of ^{235}U, which is the basis of determining fission events and the energy of incident neutrons, has however a strong resonance effect in the eV-keV energy range [11]. It could cause worse accuracy and enlarge experimental uncertainty in the neutron total cross section measurements of nuclides with resonance peaks in the same energy region. Besides, the detection efficiency of the multi-cell fission chamber is limited due the low quantities of ^{235}U while increasing ^{235}U cells is costing and challenging for data analysis. For this, a lithium-containing scintillation detector has been proposed as an upgrade spectrometer for neutron total cross section measurements due to the high and smooth cross sections of ^{6}Li(n,α)T reaction.

At GELINA, the Geel Electron LINear Accelerator facility located in Belgium, Li-glass detectors, plastic scintillators and NE213 scintillators have been applied for neutron total cross section measurements at flight paths with distances from the target up to 400 m [12, 13]. As a shadow bar made of Cu/Pb was placed close to the uranium target to reduce the γ-ray flash and the fast neutron component, background was significantly decreased for neutron measurements using those scintillators by combing with a ^{10}B overlap filter close to the sample position for slow neutrons absorption. At the photoneutron source (PNS) nELBE, a very compact neutron time-of-flight (nToF) system installed at the superconducting electron linear accelerator ELBE (Electron Linear accelerator with high Brilliance and low Emittance), a plastic scintillator (Eljen EJ-200) has been used for transmitted neutrons detection together with a 3 cm thick lead alloy ($PbSb_4$) to reduce the bremsstrahlung count rate [14, 15]. Similar spectrometers (e.g. ^{6}LiF(ZnS) scintillators used on the PNS at SINAP [16] and at the Pohang neutron facility (PNF)[17], a GS20 ^{6}Li glass scintillator at the KURNS-LINAC facility [2], and a BC404 scintillator on the weapons neutron research (WNR) facility at LANSCE [1]) have been applied for neutron total cross section measurements based on different types of scintillators by considering the neutron beam characterization and

* Corresponding author, fengs9115@gmail.com

radiation environment together with using some filters.

In general, organic scintillators are used for fast neutron detection (100 keV-MeV) and inorganic scintillators are used for measuring low energy neutrons (<100 keV). Therefore, measuring the neutron total cross section in a wide energy range (e.g. eV-MeV) usually needs more than one detector and decreases the experimental efficiency as one needs more measuring time. Moreover, experimental uncertainty analysis will be challenging especially when the results obtained in the same energy range are very different. On the other hand, the Back-n beam line is facing the spallation target directly with only a Gd filter placed in front of samples for very low neutrons absorption to avoid neutrons overlapping from different pulses. The strong γ-ray flash, which is a beam of prompt γ-rays produced at the same time with spallation neutrons, could result in any scintillator working failure in a short time duration. Taking into account the above factors, a physical design and detailed simulations of the lithium-containing scintillator in such environment is first required to fulfill the needs before constructing it for neutron total cross section measurements.

In the present work, the design criteria for the physical design were first summarized with considering the experimental requirements. The $Cs_2LiLaBr_6$ (CLLB) scintillator was proposed for the FAst Scintillator-based neutron Total cross section (FAST) spectrometer design and detailed simulations of the scintillator were performed using Geant4 for detector performance evaluation in terms of detection efficiency and neutron-γ discrimination. The conceptual design were analyzed and discussed.

II. SIMULATION OF DETECTOR RESPONSE

A. Experimental requirements and design criteria

CSNS produces neutrons by proton-induced spallation on a tungsten target. Incident protons are in two bunches, about 50 ns wide and 410 ns apart, and are accelerated through a Linac and synchrotron up to 1.6 GeV with a frequency of 25 Hz and beam power of 125 kW (from Spring 2022). The Back-n neutron beam line locates in the opposite direction of the incident proton beam to target [4]. Two experimental stations, which are about 55 m and 76 m far away from the spallation target, respectively, have been installed for nuclear data measurements, irradiation tests, detector calibrations, neutron imaging and element analysis [5].

In neutron total cross section measurements, samples are placed in the endstation 1 (ES#1) and the spectrometer is placed in the endstation 2 (ES#2) to reduce scattering neutrons from samples, as shown in Fig.1. Neutrons are well collimated before arriving at the two stations and the beam spot at the spectrometer position is available in two sizes, i.e. Φ30 mm and Φ50 mm. Considering the experimental conditions, some essential criteria and requirements must be addressed in conceptual design of the FAST spectrometer.

• Fast response under strong γ-ray flash irradiation

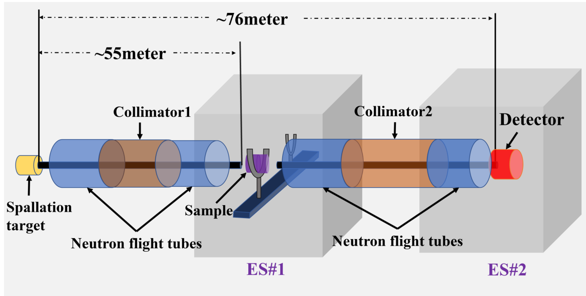

Fig. 1. Schematic view of the experimental arrangement for neutron total cross section measurements on the Back-n beam line.

The γ-ray flash has a relative strong intensity at the spectrometer position with the Φ 30 mm or Φ 50 mm neutron beam. Scintillators are usually sensitive to γ-rays and will then reach to a saturation level in a period of time for preventing the detection of after arriving fast neutrons. In this case, scintillators with fast timing response and photodetectors (e.g. photomultiplier tube (PMT) or Silicon Photomultiplier (SiPM)) with good recovery ability are required. Further more, the irradiation effect on the photodetector should be considered when placing it on the rear side of the scintillator.

• Sensitivity to both slow and fast neutrons

Lithium-containing scintillators are quite common as slow neutron detectors due to the high cross sections of ^{6}Li(n,α)T reaction in low energy range. However, the measured neutron energy spectrum of Back-n ES#2 ranging from 1 eV to 100 MeV shows a main component in MeV region [18]. In order to keep a stable response of the scintillator to both slow and fast neutrons, the ratio of ^{6}Li to ^{7}Li in lithium should be investigated for improving the experimental efficiency.

• Merit neutron-γ discrimination performance in a wide energy range

The ^{6}Li(n,α)T reaction proceeds only to the ground state of the product and the large Q-value of the reaction allows a merit discrimination of slow neutrons and γ-rays [19]. Scattering γ-rays and γ-rays produced by neutron activation on the spallation target and samples will interfere the neutron detection over the entire energy region. Therefore, the neutron-γ discrimination capability of the lithium-containing scintillator should be investigated with its thickness, geometry, scintillation property, and readout modes.

• Photodetector protection from radiation

Photodetectors coupled to the lithium-containing scintillator could be either PMTs or SiPMs. A SiPM is a matrix of avalanche photo-diodes connected in parallel with each other operating above the breakdown voltage and in Geiger mode [20]. Radiation damage is a major concern when operating these devices in harsh radiation environments [21]. Considering the high flux and high energy neutrons and γ-rays guided at ES#2, the photodetectors should be well protected from radiation. Side readout of the scintillation light could be a good choice but the light collection efficiency should be investigated to ensure that the pulse shape is smooth enough for pulse shape discrimination (PSD) analysis.

New ^{6}Li-enrich elpasolite crystals (CLYC, CLLB, CLLC, etc.) are capable of detecting both neutrons and γ-rays and discriminating them clearly [22–25]. CLLB scintillator has a higher light yield (40,000 photons/MeV) compared to other scintillators of the same type, providing a better signal shape for PSD in the side readout design (which is discussed in subsection II D 3). CLLB scintillator has a very high thermal neutron reaction cross section and can release up to 4.78 MeV energy through the ^{6}Li(n,α)^{3}H reaction, giving CLLB a good neutron response and excellent neutron-γ discrimination performance. For this reason, the CLLB scintillator has been selected as the reference for the conceptual design of the FAST spectrometer.

B. Simulation model and validation

The size of the scintillator should be large enough to cover the neutron beam in neutron total cross section measurements. As the crystal growth and fabrication process of producing a large inorganic scintillator is challenging, a CLLB scintillator with a dimension of 50.8 mm (2 inch) $\times$ 50.8 mm $\times$ 6 mm was initially considered. A CLLB model (see Fig.2) was then built in GEANT4[26, 27] to simulate its response to neutrons. A same model was also built in MCNP for validating the simulation model. The CLLB scintillator was set with a density of 4.2 g/cm^{3} and covered by a 1 mm thick aluminum shell. Simulations based on MCNP together with the ENDF/B-VIII.0 library were carried out by counting the (n,α) reaction events with the FM4 card, whereas the simulations based on the Geant4.11.1 version with the FTFP_BERT_HP physical model were performed by recording the counts of produced secondary α particles.

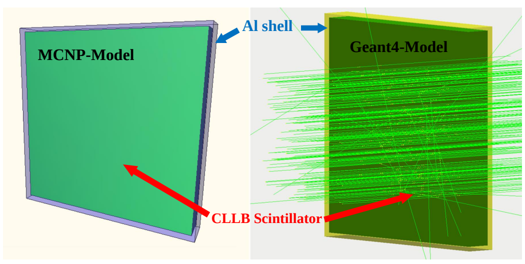

Fig. 2. Left: MCNP model; Right: Geant4 model.

Simulation results of the CLLB neutron detection efficiency using Geant4 and MCNP were compared with each other, as shown in Fig.3. The ratios of the results simulated by Geant4 to MCNP (G/M in following) were nearly the same, which indicates that calculated detection efficiencies were well matched when the statistics were high enough. Some small drops were found on the detection efficiency curve in eV-keV region, which were mainly caused by competing reaction on Cs, La and Br in the CLLB scintillator.

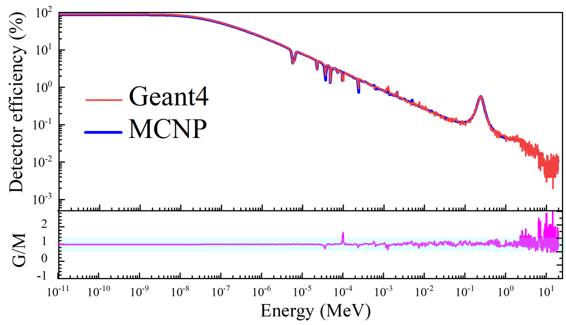

Fig. 3. Comparison of the CLLB neutron detection efficiency using Geant4 (red line) and MCNP (blue line)

C. Detection efficiency

To minimize the effect induced by γ-ray flash on CLLB, the γ-ray detection efficiency of the CLLB must be reduced. The scintillator should be thin enough while the neutron detection efficiency is limited at the same time. The energy deposition response of the CLLB scintillator to neutrons and γ-rays with different thicknesses and ratios of ^{6}Li/^{7}Li abundance were evaluated. Fig.4 shows a comparison of CLLB neutron detection efficiency with different ratios of ^{6}Li/^{7}Li abundance, which confirms that increasing the ^{6}Li enrichment improves the neutron detection efficiency significantly over the entire energy range. In order to improve the neutron detection efficiency, the ^{6}Li abundance should be higher than 90%. 95% ^{6}Li enrichment was set in following simulations.

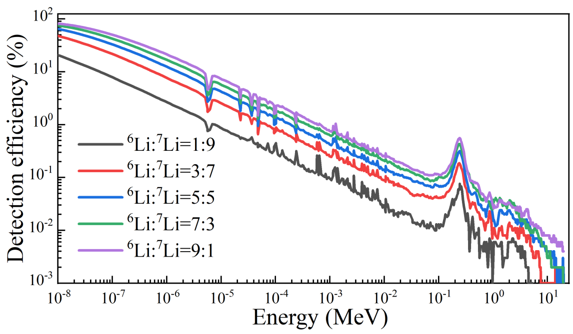

Fig. 4. Detection efficiency simulation results as a function of neutron energy with different ratios of ^{6}Li/^{7}Li abundance

Fig.5 shows the simulation results of the CLLB response to Back-n neutrons and γ-rays by multiplying the detection efficiency and the original energy spectra at the spectrometer position (ES#2). Neutron counts have considered the (n, α) reactions only and the γ-ray detection efficiency corresponds to the peak detection efficiency. The in-beam γ-ray energy spectrum was extracted from reference [28]. The neutron detection efficiency of CLLB decreases exponentially with neutron energy, as shown in Fig.4. However, as keV-MeV neutrons contribute the main component on the neutron energy spectrum (black dash line shown in Fig.5 (Up)), the response of CLLB to neutrons on the Back-n beam line changes not sig-

nificantly over the entire energy range. Fig.5 (Down) shows a similar simulation with the in-beam γ-ray energy spectrum of Back-n (black dash line). The response of CLLB to γ-rays on the Back-n beam line drops rapidly as a function of energy. The γ-ray detection efficiency of CLLB was calculated to be sensitive to thickness and thin scintillators (3-6 mm) were found having a detection efficiency 1-2 orders lower than thick ones (12-21 mm).

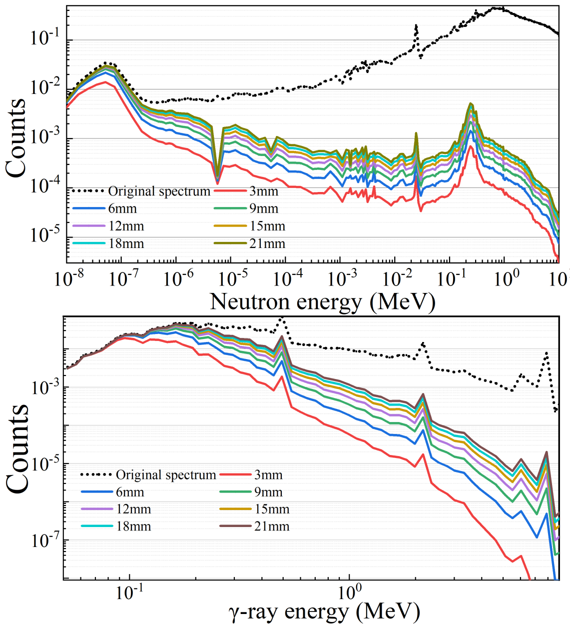

Fig. 5. Simulation results of the CLLB response to Back-n neutrons and γ-rays with different thicknesses. Up: Response to the neutron spectrum; Down: Response to γ-ray energy spectrum.

In order to identify a suitable thickness for compromising high neutron detection and low γ-ray detection, the ratio of detected neutrons to γ-rays (n/γ in following) as a function of time-of-flight (ns) was calculated with different CLLB thicknesses, as shown in Fig.6. Double bunch structure of the neutron beam has been considered. The neutron TOF spectrum was first derived from the neutron energy spectrum extracted from reference [4], and then obtained by summing the two idetifical TOF spectrum with a time interval of 410 ns. The double bunch structure of γ-ray TOF spectrum was extracted from [28]. n/γ was the neutron TOF spectrum divided by the γ-ray TOF spectrum (dash line) and considering the CLLB detection efficiency to neutrons and γ-rays (solid lines). Fig.6 shows that the detected n/γ decreases with neutron energy while keeps a relative stable level with CLLB thickness. Considering that the high intensity γ-ray flash is followed by high energy neutrons, low detection efficiency to γ-rays will be better and a thin CLLB scintillator (e.g. 3 mm) will be a preferring choice for γ-rays suppression. Even the CLLB scintillator containing high enriched ^{6}Li has been proposed for high detection efficiency, its capability of neutron-γ discrimination needs to be investigated.

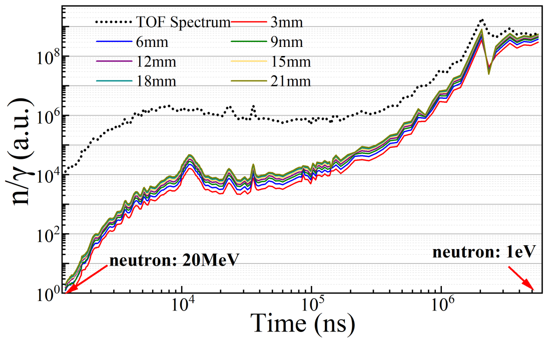

Fig. 6. n/γ ratios of CLLB response to neutrons and γ-rays with different thicknesses and original spectrum

D. Neutron-γ discrimination

1. *Pulse shape simulation*

In a typical pulse generated by the CLLB scintillator, the decay component of the scintillation light can usually be described by the sum of two exponential functions, as shown in Equation 1.

$$I(t) = I_f e^{\frac{-t}{\tau_f}} + I_s e^{\frac{-t}{\tau_s}} \tag{1}$$

Where I_s and I_f are the scintillation intensities of slow and fast components, respectively, and τ_s and τ_f are decay time constants of slow and fast components. Secondary charged particles produced by neutrons and γ-rays have different ionisation energy loss rates (-dE/dx), resulting in the luminescence decay curves with different fast and slow components for PSD of neutrons and γ-rays, as shown in Fig.7.

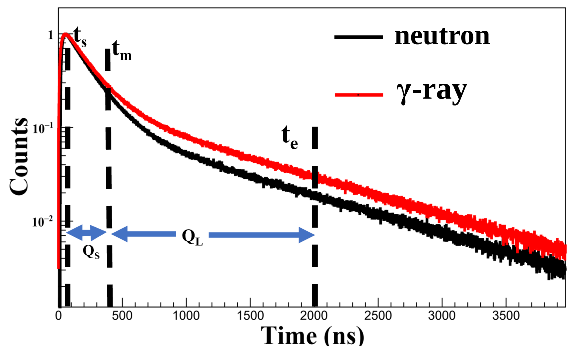

Fig. 7. A typical simulated neutron pulse compared with a normalized γ-ray pulse

Simulation of the pulse shape of scintillation light as a function of time was performed as Geant4 contains the physical process for optical photon transportation [29]. A reflective layer was built with an Aluminum foil covering the CLLB scintillator. In optical simulations, the optical characteristics of various materials must be specified. A quartz glass

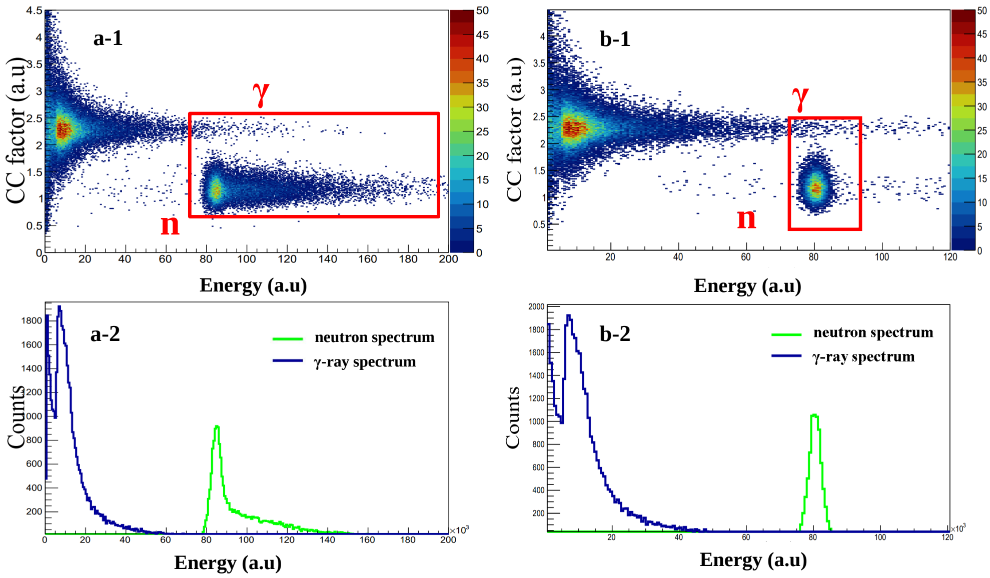

Fig. 8. 2D histograms of the neutron-γ discrimination (up) and corresponding energy spectra (down). Left panel: without a HDPE moderated Cf-252 source; Right panel: with a HDPE moderator.

window and a photocathode material were added to the light output surface, allowing optical photons to be transported through the quartz glass window to the photocathode and to be converted into electrons through the photoelectric effect. The light emission spectrum of CLLB was extracted from the work performed by Urmila Shirwadkar, et al [30]. The refractive index and absorption length curve for all materials as a function of photon wavelength was inserted using the AddPropery function. More physical parameters of CLLB scintillator was set via the AddConstPropery function, namely the light yield (40,000 photons/MeV), fast (180 ns) and slow (1080 ns) decay time, and the ratios of fast to slow components for neutrons (50:50) and γ-rays (61:39). The interface between different materials and the optical properties of interface was set [29], including the surface types, models, finishes and reflection (e.g. the surface type between the aluminum shell and the CLLB crystal was set as dielectric_metal, the surface model was set to glisur model, the finishes was set to polished, and reflectivity was set to 1).

A typical surface Cf-252 source with a diameter of 50 mm was built to generate neutrons and γ-rays. The γ-ray and neutron emission spectrum can be described by Equation (2) and Maxwell's distribution [31], respectively. A 4 mm thick high density polyethylene (HDPE) was adopted to slow down fast neutrons for a high detection efficiency to neutrons.

$$f(E) = \begin{cases} 38.13E_n e^{1.648E_n} & E_n \leq 0.3 \\ 26.8E_n e^{-2.3E_n} & 0.3 < E_n \leq 1.0 \\ 8.0E_n e^{-1.1E_n} & E_n > 1 \end{cases} \quad (2)$$

The simulation of the light pulse of each event was obtained by counting the time distribution of all photons arriving at the photocathode. In order to simulate the electric pulse, the number of photons within each time bin of the light pulse was converted to the number of electrons by calculating the convolution of the photon energy distribution and the photon detection efficiency curve of the photocathode. The quantum efficiency of a HAMAMATSU MPPC-S14160 SiPM was applied here. A typical simulated neutron pulse compared with an amplitude-normalizing γ-ray pulse is shown in Fig.7.

2. *PSD analysis*

The simulated neutron-γ discrimination performance of the CLLB scintillator was evaluated based on the PSD analysis. The Charge Comparison (CC) [32] method was applied for comparing the charge differences over the tail of pulses by calculating the CC factor as a function of Energy. The CC factor was the ratio of a long integration Q_L from t_m to t_e to a short integration Q_S from t_s to t_e of the pulse, as illustrated in Fig.7. The Figure of merit (FoM) [33] was defined as Equation (3) for quantitative evaluation.

$$FoM = \frac{S}{FWHM_n + FWHM_\gamma} \quad (3)$$

Where S is the separation between two peaks contributed by neutrons and γ-rays, $FWHM_n$ and $FWHM_\gamma$ represent the full width at half maximum (FWHM) of two peaks, respectively.

Fig.8 shows the 2D histograms of the neutron-γ discrimination and the corresponding neutron and γ-ray pulse height spectrum without and with a 4 cm thick HDPE moderator, respectively. The distribution of fast neutron events is continuum, with a response of 4.78 MeV plus incident fast neutron kinetic energy, whereas the distribution of thermal neutron

events is concentrated at around 4.78 MeV. Similar experimental result was found in reference [34] on the ^{6}Li(n, α) reaction response and PSD performance of a CLYC scintillator. The CLLB scintillator shows an excellent PSD performance with a FoM value of 1.46 for fast neutrons and 1.42 for moderated neutrons, respectively, as cutting the red area for events selection shown in Fig.8.

3. *Analysis of influencing factors on PSD performance*

• Scintillator shape and thickness

Cylindrical inorganic scintillator is commonly applied for commercial use and is usually coupled by a photodetector detecting scintillation light from the rear side. Cubic scintillator is easier for side readout while the light collection efficiency and uniformity should be investigated. In order to compare the PSD performance with different scintillator shapes and thicknesses, neutron-γ discrimination performance of a cylindrical scintillator (Φ 50.8 mm) and a cubic scintillator (50.8 mm $\times$ 50.8 mm) with different thicknesses were simulated and analyzed. Fig.9 shows the FoM values as a function of thickness for cylindrical and cubic scintillators, revealing that the PSD performance of the cubic scintillator is well in consistent with the cylindrical one. FoM values are found increasing significantly from 2 mm to 4 mm and then go to a slow increasing level. The main reason could be that the thermal neutron absorption length of the high ^6Li-enriched CLLB scintillator is about 3 mm [35]. Considering the required PSD quality in low energy range, the thickness of the CLLB scintillator should be larger than 3 mm.

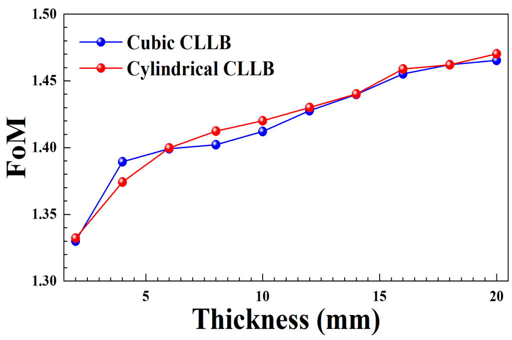

Fig. 9. FoM results as a function of the CLLB thickness with different shape.

• Shares of fast and slow scintillation component

It was found that changing the share of the fast component of CLLB scintillation light has a significant impact on its PSD performance [36]. Fig.10 shows the relative position distribution of neutrons and γ-rays in the 2D histogram of PSD when different fast scintillation components were set for neutrons and γ-ray, respectively. Fig.10 (a-f) correspond to the PSD simulation results with changing the fast scintillation component shares (40%-90%) for neutrons only. A large fast component of the scintillation light generated by neutrons could improve PSD significantly, as shown in Fig.11 (black line). On the contrary, the performance of PSD decreases rapidly with increasing the share of fast scintillation component for γ-rays, as shown as the red line, which was obtained by using the simulation results shown in Fig.10 (g-l). Accurate shares of fast and slow component of the scintillation light generated by neutrons and γ-ray are proved to be critical in PSD simulation, which provides a reference for achieving a better PSD performance in elpasolite crystals design.

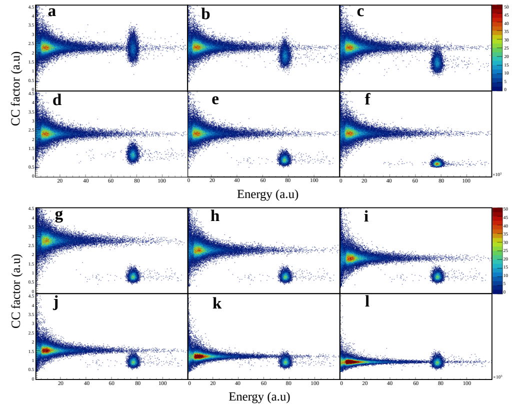

Fig. 10. 2D histogram of simulated neutron-γ discrimination with different fast component shares in pulses generated by neutrons (upper panel) and γ-rays (bottom panel). a-f: shares ranging from 40% to 90% with an interval of 10%; g-l: shares ranging from 30% to 80% with an interval of 10%.

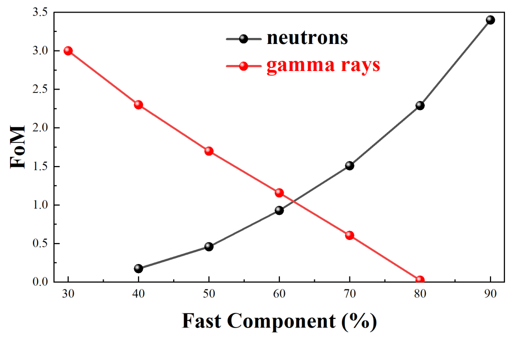

Fig. 11. FoM results as a function of fast component ratio of neutron and γ-ray respectively.

• Readout modes

In order to protect the photodetector from the irradiation of high intensity of neutrons and γ-rays, side readout is prior to rear readout for consideration in physical design of the FAST spectrometer. Scintillation light collection and PSD performance were calculated with different readout modes using a moderated Cf-252 neutron source. Fig.12 shows the models built in Geant4 and the corresponding 2D histogram of PSD performance, from which it can be noted that the side readout mode collects fewer photons than the rear readout. This is because the photons have a longer transportation path

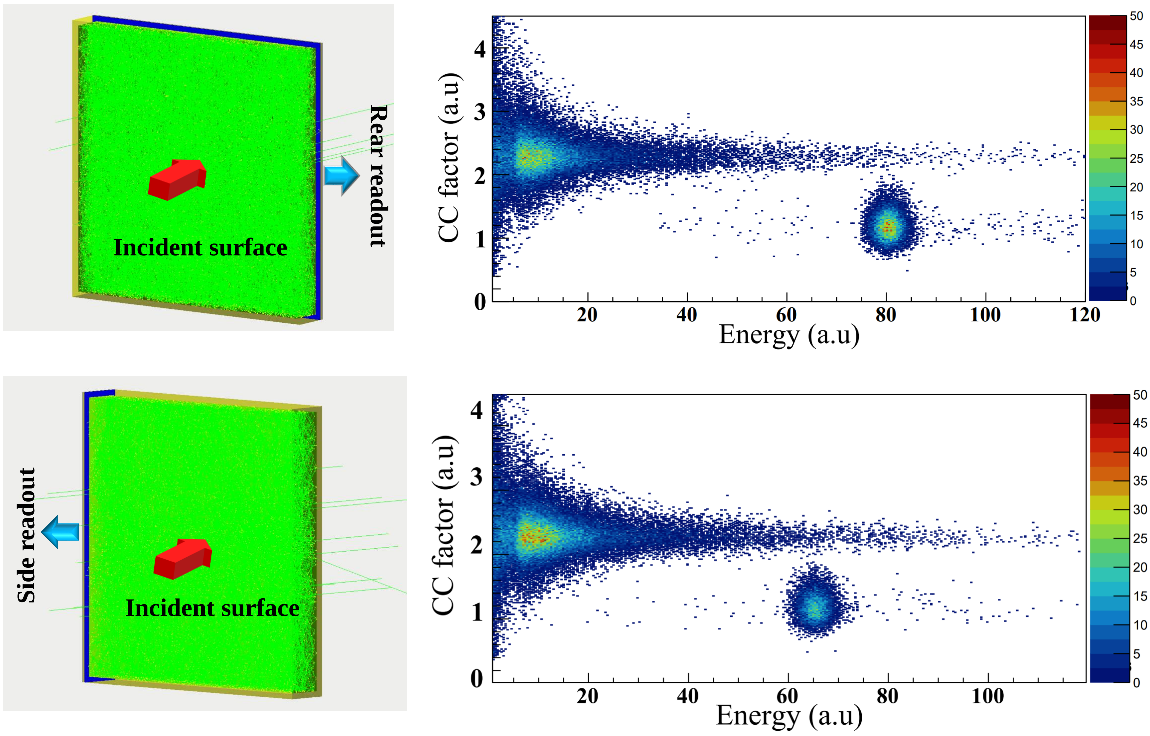

Fig. 12. Comparison of scintillation light collection models and the corresponding 2D histograms of PSD simulations with rear readout (Up) and side readout (Down).

through the scintillator in the side readout model and the collecting area is also lower than that in the rear readout model, resulting in some optical photons being self-absorbed by the scintillator itself. However, the PSD performances of the two model were comparable, showing a FoM of 1.44 with the rear readout compared with a FoM of 1.42 with the side readout model.

III. DISCUSSIONS

The physical design of a CLLB scintillator-based spectrometer for neutron total cross section measurements includes determining the readout mode and physical parameters of the scintillator, i.e. scintillator area, thickness, ^{6}Li enrichment, Ce-doping percentage, and PSD performance in the interest energy range. With calculations performed using the Geant4 code on detection efficiency to neutrons, a high ^{6}Li-enriched (>90%) CLLB scintillator has been proposed for a higher neutron detection efficiency in 1 eV to 10 MeV energy range. A thin CLLB scintillator is a preferred choice based on the calculations on n/γ ratios of CLLB response to neutrons and γ-rays with considering the Back-n neutron and γ energy spectra. However, thin CLLB scintillators have worse neutron-γ discrimination performance. As a compromise, a 4-9 mm thick CLLB scintillator has been recommended for the FAST spectrometer design but the final size depends on the crystal growth and fabrication level as well. For achieving a better neutron-γ discrimination performance, the fast component of scintillation light generated by neutrons should be as high as possible while γ-rays require a low fast scintillation component. The share of fast component in scintillation light generated by neutrons can be adapted with Ce doping percentage [36]. As the PSD performance changes slightly with side readout compared with rear readout, an array of SiPMs is designed coupling to the side of a CLLB scintillator for radiation protection. The inherent fast rise time of the SiPM due to the avalanche characteristics of the pixels makes it ideal for counters in TOF spectrometers [37, 38]. In reality, a gated technique [39] and a shadow bar could also be applied for spectrometer response recovery and γ-ray flash reduction. In future, a calibration experiment based on a neutron generator should be performed for the validation of the simulations dedicated for the physical design of the FAST spectrometer.

IV. CONCLUSIONS

In order to design a FAst Scintillator-based neutron Total cross section spectrometer (FAST) on the Back-n beam line at CSNS, a detailed simulation of the CLLB response to neutrons and γ-rays was performed using the Geant4 toolkit. The detection efficiency of a CLLB scintillator was investigated as a function of ^{6}Li abundance and a high ^{6}Li-enriched (95%) CLLB scintillator was then applied for simulations on thickness investigation and PSD performance. The PSD performances of different thick CLLB scintillators were simulated with a standard Cf-252 neutron source and the quan-

tum efficiency curve of a commercial SiPM. The influences resulted by different shapes, thicknesses, shares of fast component in scintillation ligh, and readout modes were simulated and analyzed. As a result, a final conceptual design of the FAST spectrometer has been proposed based on a 50.8 mm $\times$ 50.8 mm cubic scintillator to cover the Φ50 mm neutron beam line on the Back-n beam line. The cubic CLLB is high ^{6}Li-enriched (>90%), 4-9 mm thick, and capable of high neutron-γ discriminating performance (FoM>1.3 for thermal neutrons). An array of SiPMs coupled to the CLLB scintillator with side readout is considered for radiation protection and a benchmarking experiment for validating simulations with a neutron generator has been recommended in future. The simulations, especially the technique of pulse shape simulation developed for PSD analysis, support the construction of the FAST spectrometer and provide an important reference for similar spectrometer design on the Back-n beam line.

V. ACKNOWLEDGMENTS

This work was supported by the Key Laboratory of Nuclear Data foundation (JCKY2022201C153), the National Natural Science Foundation of China (Grant No. 11505216), the Educational Commission of Hunan Province of China (19B488) and the Natural Science Foundation of Hunan Province of China (2021JJ40444, 2020RC3054).

[1] W. P. Abfalterer, F. B. Bateman, F. S. Dietrich, et al., Measurement of neutron total cross sections up to 560 MeV, Phys. Rev. C 63 (4), 044608 (2001). https://doi.org/10.1103/PhysRevC.63.044608

[2] Jaehong Lee, Jun Nishiyama, Jun-Ichi Hori et al., Neutron total cross section measurements of polyethylene using time-of-flight method at KURNS-LINAC, J. Nucl. Sci. Technol. 57 (1), 1–8 (2020). https://doi.org/10.1080/00223131.2019.1647894

[3] S. Kopecky, P. Riehs, J. A. Harvey et al., New Measurement of the Charge Radius of the Neutron. Phys. Rev. Lett. 74 (13), 2427 (1995). https://doi.org/10.1103/PhysRevLett.74.2427

[4] Qi An, HY Bai, Jie Bao, et al., Back-n white neutron facility for nuclear data measurements at CSNS. J. Instrum. 12 (07), P07022 (2017). https://doi.org/10.1088/1748-0221/12/07/P07022

[5] Tang. JY, An. Q, Bai. JB. et al. Back-n white neutron source at CSNS and its applications. Nucl. Sci. Tech. 32, 11 (2021). https://doi.org/10.1007/s41365-021-00846-6

[6] J. Wen, Y. Yang, Z. Wen et al., A multi-layered fast ionization chamber prototype for fission cross section measurements. J. Instrum. 13 (07), P07020 (2018). https://doi.org/10.1088/1748-0221/13/07/P07020

[7] Y. Yang, Z. Wen, Z. Han et al., A multi-cell fission chamber for fission cross-section measurements at the back-n white neutron beam of CSNS. Nucl. Instr. Methods A 940, 486–491 (2019). https://doi.org/10.1016/j.nima.2019.06.014

[8] X.Y. Liu, Y.W. Yang, R.Liu et al., Measurement of the neutron total cross section of carbon at the back-n white neutron beam of CSNS. Nucl. Sci. Tech. 30 (9), 1–10 (2019). https://doi.org/10.1007/s41365-019-0660-9

[9] X. Liu, Y. Yang, R. Liu et al., Measurement of the neutron total cross sections of aluminum at the back-n white neutron source of CSNS. Eur. Phys. J. A 57 (7), 1–11 (2021).https://doi.org/10.1140/epja/s10050-021-00513-9

[10] Jiang-Lin Zhang, Bing Jiang, Yong-Hao Chen et al., Measurement of total neutron cross section of natural lithium at China Spallation Neutron Source Back-n facility, Acta Phys. Sin. 71 (5), 052901 (2022). https://doi.org/10.7498/aps.71.20211646

[11] Zhigang Ge, Ruirui Xu, Haicheng Wu et al., CENDL-3.2: The new version of Chinese general purpose evaluated nuclear data library, EPJ Web Conf. 239, 09001 (2020). https://doi.org/10.1051/epjconf/202023909001

[12] W Mondelaers, P Schillebeeckx, GELINA, a neutron time-of-flight facility for high-resolution neutron data measurements, Research Infrastructures (2), 19–25 (2006). https://publications.jrc.ec.europa.eu/repository/handle/JRC35644

[13] I Sirakov, B Becker, R Capote et al., Results of total cross section measurements for ^{197}Au in the neutron energy region from 4 to 108 keV at GELINA, Eur. Phys. J. A 49, 144 (2013). https://doi.org/10.1140/epja/i2013-13144-2

[14] Roland Hannaske, Zoltan Elekes, Roland Beyer et al., Neutron total cross section measurements of gold and tantalum at the nELBE photoneutron source, Eur. Phys. J. A 49, 137 (2013). https://doi.org/10.1140/epja/i2013-13137-1

[15] Arnd Junghans, Roland Beyer, Jürgen Claußner et al., Neutron transmission measurements at nELBE, EPJ Web Conf. 239, 01006 (2020). https://doi.org/10.1051/epjconf/202023901006

[16] LX Liu, HW Wang, YG Ma et al., Measurements of the total cross section of ^{nat}Be with thermal neutrons from a photo-neutron source, Nucl. Instr. Methods B 410, 158–163 (2017). https://doi.org/10.1016/j.nimb.2017.08.022

[17] S. G. Shin, Y.-U. Kye, M.-H. Cho et al., Neutron total cross-section measurements with the ^{6}Li-Zns (Ag) scintillator (BC702) employing a neutron and noise separation technique. J. Korean Phys. Soc. 64 (9), 1288–1292 (2014). https://doi.org/10.3938/jkps.64.1288

[18] Yonghao Chen, Guangyuan Luan, Jie Bao et al., Neutron energy spectrum measurement of the Back-n white neutron source at CSNS, Eur. Phys. J. A 55, 115 (2019). https://doi.org/10.1140/epja/i2019-12808-1

[19] Glenn F. Knoll, Radiation detection and measurement (fourth edition). John Wiley & Sons (2010)

[20] E. Garutti, Yu. Musienko, Radiation damage of SiPMs, Nucl. Instr. Methods A 926, 69–84 (2019). https://doi.org/10.1016/j.nima.2018.10.191

[21] B Biró, G. David, A. Fenyvesi et al., A Comparison of the Effects of Neutron and Gamma Radiation in Silicon Photomultipliers, IEEE Trans. Nucl. Sci. 66 (7), 1833–1839 (2019). https://doi.org/10.1109/TNS.2019.2921102

[22] J. Glodo, E. van Loef, R. Hawrami et al., Selected properties of Cs_2LiYCl_6, $Cs_2LiLaCl_6$, and $Cs_2LiLaBr_6$ scintillators. IEEE Trans. Nucl. Sci. 58 (1), 333–338 (2011). https://doi.org/10.1109/TNS.2010.2098045

[23] R. S. Woolf, E. A. Wulf, B. F. Phlips et al., Identification of internal radioactive contaminants in elpasolites (CLYC, CLLB, CLLBC) and other inorganic scintillators. Nucl. Instr. Methods A 954, 161228 (2020). https://doi.org/10.1016/j.nima.2018.09.063

[24] J. Glodo, R. Hawrami, E. van Loef et al., Pulse shape discrimination with selected elpasolite crystals. IEEE Trans. Nucl. Sci. 59 (5), 2328–2333 (2012). https://doi.org/10.1109/TNS.2012.2188646

[25] K.-N. Li, X.-P. Zhang, Q. Gui et al., Characterization of the new scintillator Cs_2LiYCl_6: Ce3+. Nucl. Sci. Tech 29 (1), 1–6 (2018). https://doi.org/10.1007/s41365-017-0342-4

[26] S. Agostinelli, J. Allison, K. a. Amako et al., GEANT4—a simulation toolkit. Nucl. Instr. Methods A 506 (3), 250–303 (2003). https://doi.org/10.1016/S0168-9002(03)01368-8

[27] J Allison, K Amako, J Apostolakis, et al., Recent developments in Geant4. Nucl. Instr. Methods A 835, 186–225 (2016). https://doi.org/10.1016/j.nima.2016.06.125

[28] Jie Ren, Xi-Chao Ruan, Yong-Hao Chen et al., In-beam γ-rays of back-streaming white neutron source at china spallation neutron source. Acta Phys. Sin. 69 (17), 20200718 (2020). https://doi.org/10.7498/aps.69.20200718

[29] E. Dietz-Laursonn, Peculiarities in the simulation of optical physics with Geant4, arXiv preprint arXiv:1612.05162 2016. https://doi.org/10.48550/arXiv.1612.05162

[30] U. Shirwadkar, J. Glodo, E. V. Van Loef et al., Scintillation properties of $Cs_2LiLaBr_6$(CLLB) crystals with varying Ce3+ concentration. Nucl. Instr. Methods A 652 (1), 268–270 (2011). https://doi.org/10.1016/j.nima.2010.08.050

[31] J. Meadows, Cf 252 fission neutron spectrum from 0.003 to 15.0 MeV. Phys. Rev 157 (4), 1076 (1967). https://doi.org/10.1103/PhysRev.157.1076

[32] D. Zhao, S. Feng, C. Hu et al., Characterization of the neutron/γ-ray discrimination performance in an EJ-301 liquid scintillator for application to prompt fission neutron spectrum measurements at CSNS. Radiat. Meas. 151, 106703 (2022). https://doi.org/10.1016/j.radmeas.2022.106703

[33] H. Arahmane, EM. Hamzaoui, Y. Ben Maissa et al., Neutron-gamma discrimination method based on blind source separation and machine learning. Nucl. Sci. Tech. 32, 18 (2021). https://doi.org/10.1007/s41365-021-00850-w

[34] N. D'olympia, P. Chowdhury, C. Lister et al., Pulse-shape analysis of CLYC for thermal neutrons, fast neutrons, and gamma-rays. Nucl. Instr. Methods A 714, 121–127 (2013). https://doi.org/10.1016/j.nima.2013.02.043

[35] P. R. Menge, J. Lejay, V. Ouspenski, Design and performance of a compact $Cs_2LiLaBr_6$(Ce) neutron/gamma detector using silicon photomultipliers. IEEE Nucl. Sci. Symp. Med. Imaging Conf. Rec. 1–5 (2015). https://doi.org/10.1109/NSSMIC.2015.7581858

[36] K. Yang, P. R. Menge, J. Lejay et al., Scintillation properties and temperature responses of $Cs_2LiLaBr_6$: Ce 3+. IEEE Nucl. Sci. Symp. Med. Imaging Conf. Rec. 1–6 (2013). https://doi.org/10.1109/NSSMIC.2013.6829676

[37] Q. Wang, X. Tuo, C. Deng et al., Characterization of a Cs_2LiYCl_6: Ce3+ scintillator coupled with two silicon photomultiplier arrays of different sizes. Nucl. Instr. Methods A 942, 162339 (2019). https://doi.org/10.1016/j.nima.2019.162339

[38] F. Liang and J. Smith, Characterization of CLLBC coupled to silicon photomultipliers. IEEE Trans. Nucl. Sci. 67 (6), 927–932 (2020). https://doi.org/10.1109/TNS.2020.2988555

[39] Po Hu, Zhi-Guo Ma, Kai Zhao et al., Development of gated fiber detectors for laser-induced strong electromagnetic pulse environments. Nucl. Sci. Tech. 32, 58 (2021). https://doi.org/10.1007/s41365-021-00898-8